# Probing the Co Role for Promoting OER and Zn-Air Battery Performance of NiFe-LDH: A Combined Experimental and Theoretical Study

Shilong Liu,[a, b, #] Rendian Wan,[a, b, #] Zongshan Lin,[a, b] Zhe Liu,[a] Yonggang Liu,[a] Yong Tian,[b,*] Dong-Dong Qin, [c,*] and Zhenghua Tang [a,d,*]

[a.] Guangzhou Key Laboratory for Surface Chemistry of Energy Materials and New Energy Research Institute, School of Environment and Energy, South China University of Technology, Guangzhou Higher Education Mega Centre, Guangzhou, 510006, China.

E-mail: zhht@scut.edu.cn

[b.] School of Pharmacy, Guangdong Pharmaceutical University, Guangzhou, 510006, P. R. China.

E-mail: tian_yong_tian@163.com

[c.] College of Chemistry and Chemical Engineering, Guangzhou University, 230 Wai Huan Xi Road, Guangzhou Higher Education Mega Center, Guangzhou, 510006, China.

E-mail: ccqindd@gzhu.edu.cn

[d.] State Key Laboratory of Subtropical Building Science, South China University of Technology, Guangzhou, 510640, China

#: These two authors contributed equally.

**Calculation of electrochemically active surface area (EASA), turnover frequency (TOF), and mass activity (MA):**

The EASA of the sample was estimated from the electrochemical double-layer capacitance ($C_{dl}$) of the catalyst. The $C_{dl}$ was measured via cyclic voltammograms with a potential range where no apparent Faradaic process was taking place. The double-layer charging current $I_c$ can be related to the scan rates through **Equation S1**:

$$I_c = C_{dl} \times v$$

**Equation S1**

Thus, plotting the charging currents at a specific potential against various scan rates leads to a straight line with the slope equal to $C_{dl}$ (**Figure S7**). Subsequently, the EASA value can be obtained by **Equation S2**:

$$EASA = \frac{C_{dl}}{C_s}$$

**Equation S2**

where $C_s$ is the specific capacitance of the catalyst. Here, we use general specific capacitances of $C_s = 0.040$ mF·cm$^{-2}$ based on typical reported values.

The TOF and MA values of the catalyst were calculated by following the equations in previous report.

$$MA = \frac{j}{m}$$

**Equation S3**

where $j$ (mA·cm-2 geo) is the measured current density at various overpotential.

$$TOF = \frac{j \times A}{4 \times F \times n}$$

**Equation S4**

where $j$ (mA·cm-2 geo) is the measured current density at various overpotential, $A$ (0.25 cm$^2$) is the area of the glass carbon electrode, $F$ is Faraday's constant (96485.4 C·mol$^{-1}$) and $n$ is the moles of the metal atom on the electrode. In this work, we assumed that all metal atoms were catalytically active no matter whether they are accessible to the electrolyte or not according to the reported literature.

**Calculation of Tafel plots：**

Tafel slope is an important criterion to evaluate the catalytic kinetics of the catalyst, and the Tafel slope values can be obtained by fitting the linear portions of the Tafel plots according to the following equation:

$$\eta = b\log j + a$$

**Equation S5**

where η, j, b, and a is the overpotential (V), current density (mA cm$^{-2}$), Tafel slope (mV dec$^{-1}$), and an analyzed constant, respectively.
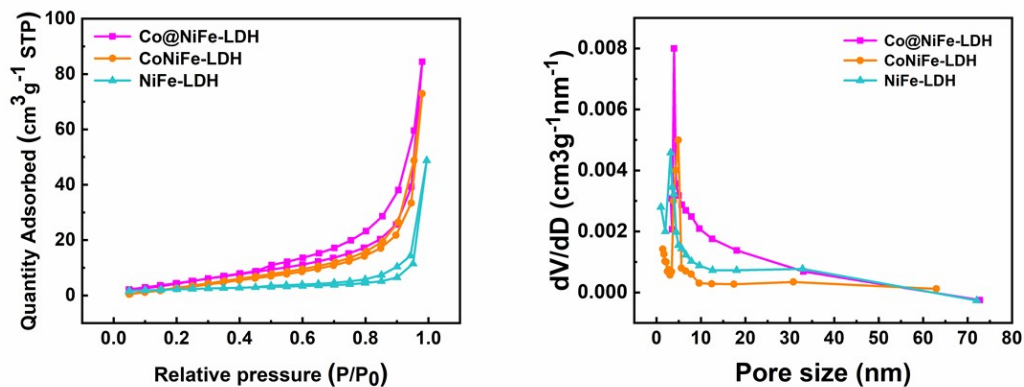
**Supplementary Figures**



**Figure S1.** (a) The $N_2$ adsorption/desorption isotherms and (b) pore size distribution for various samples.
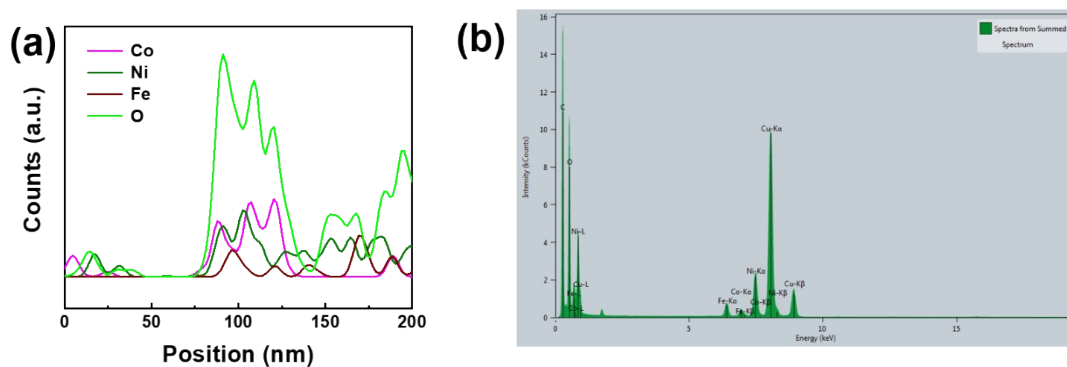


**Figure S2.** (a) EDS line-scanning profile and (b) EDS spectra of the Co@NiFe-LDH sample (the C and Cu signals are from the TEM carbon film with copper grids).
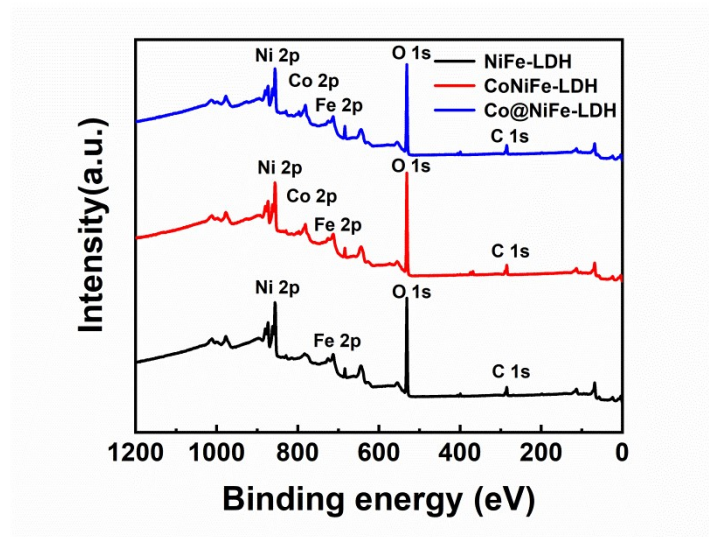
**Figure S3.** XPS survey scan spectra of NiFe-LDH, CoNiFe-LDH, and Co@NiFe-LDH.
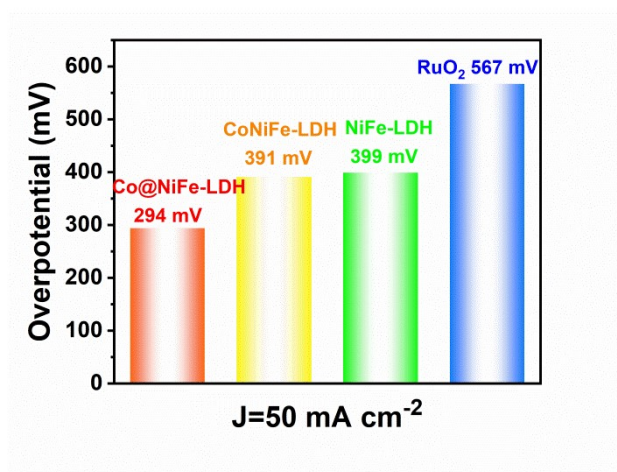


**Figure S4.** The overpotential @ 50 mA cm$^{-2}$ for NiFe-LDH, CoNiFe-LDH, Co@NiFe-LDH, and RuO$_2$ in 1 M KOH.
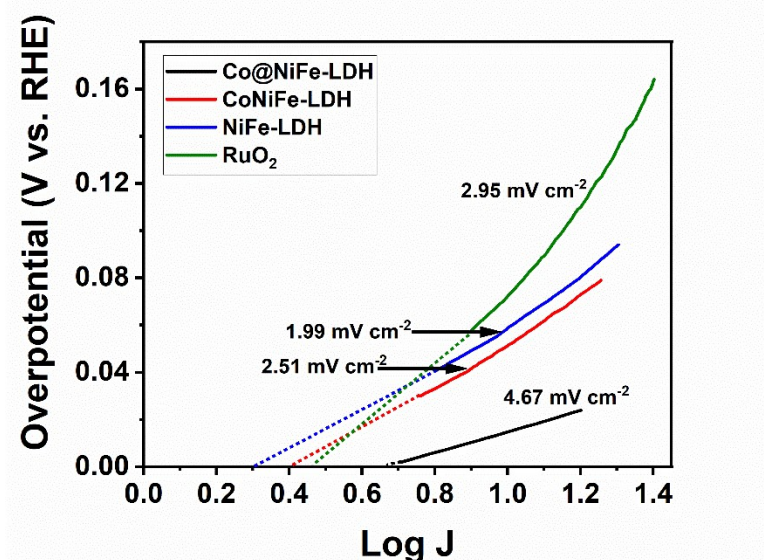
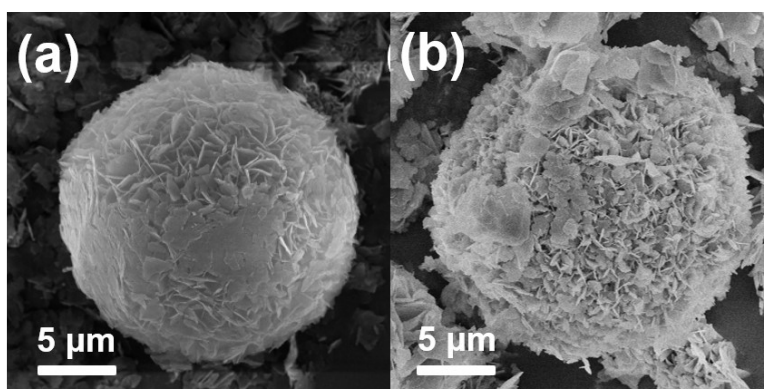**Figure S5.** Exchange current densities of the electrocatalysts.



**Figure S6.** Representative SEM image of Co@NiFe-LDH after the stability test for 20 h in 1 M KOH(a) (b).
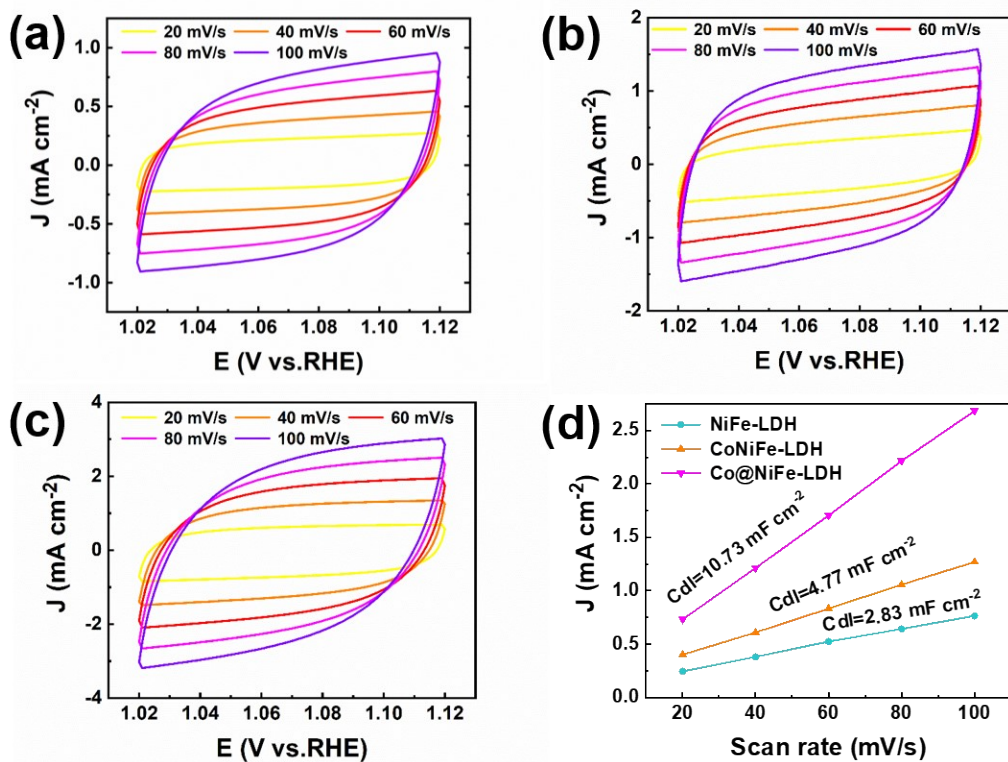
**Figure S7.** Cyclic voltammograms of (a) NiFe-LDH, (b) CoNiFe-LDH, and (c) Co@NiFe-LDH in the region of 1.02-1.12 V in 1.0 M KOH at various scan rates and (d) The plots of current density as a function of scan rate derived from (a-c), respectively.
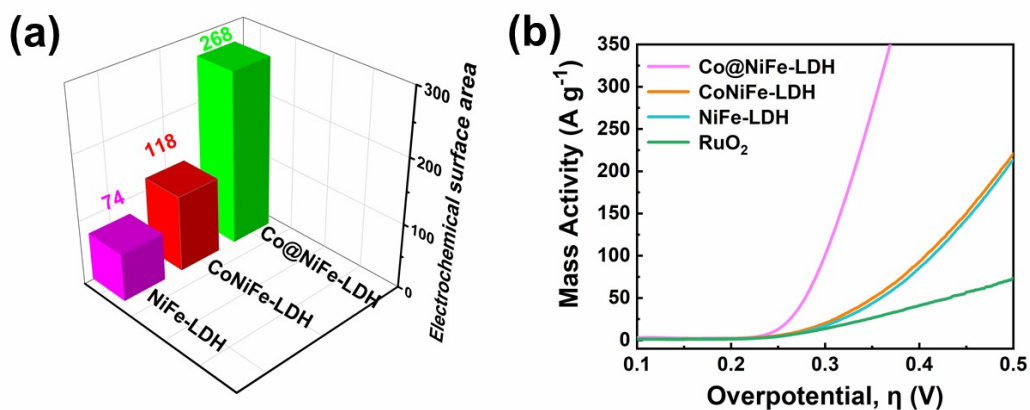


**Figure S8.** (a) The electrochemically active surface area of different catalysts in OER test. (b) Mass activity for various catalysts in OER test.
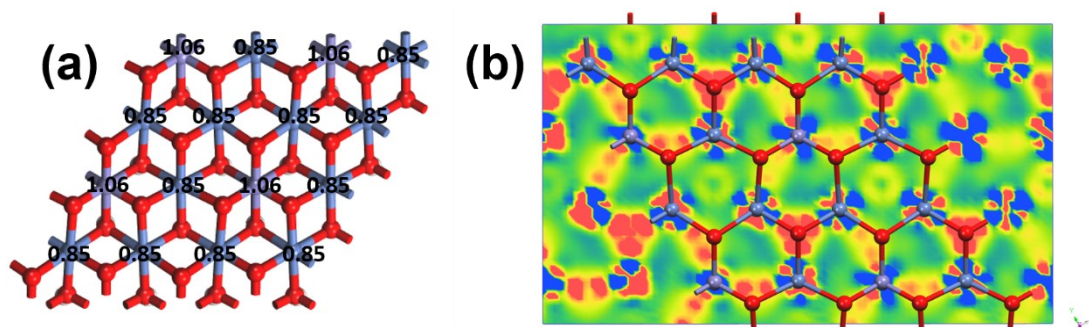
**Figure S9.** (a) The Bader charge numbers of atoms in NiFe-LDH. (b) Differential charge density of NiFe-LDH (the red contour represents the charge accumulation).
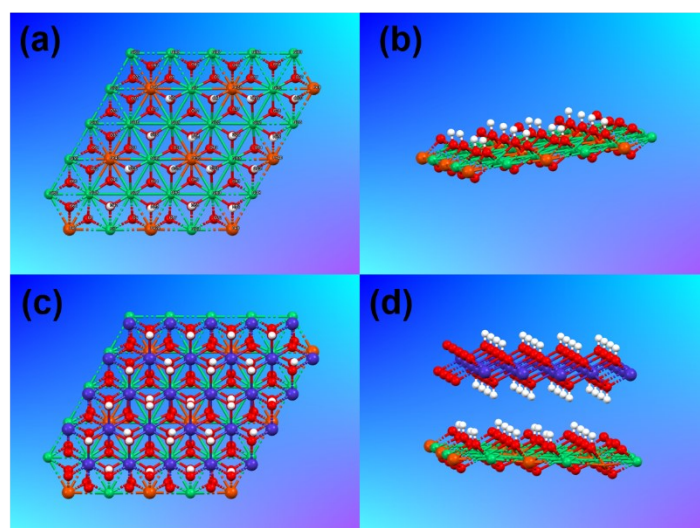


**Figure S10**. Top view of (a) NiFe-LDH model and (c) Co@NiFe-LDH model, side view of (b) NiFe-LDH model and (d) Co@NiFe-LDH model (Green, orange, red, purple, and white spheres depict Ni, Fe, O, Co, and H atoms, respectively).

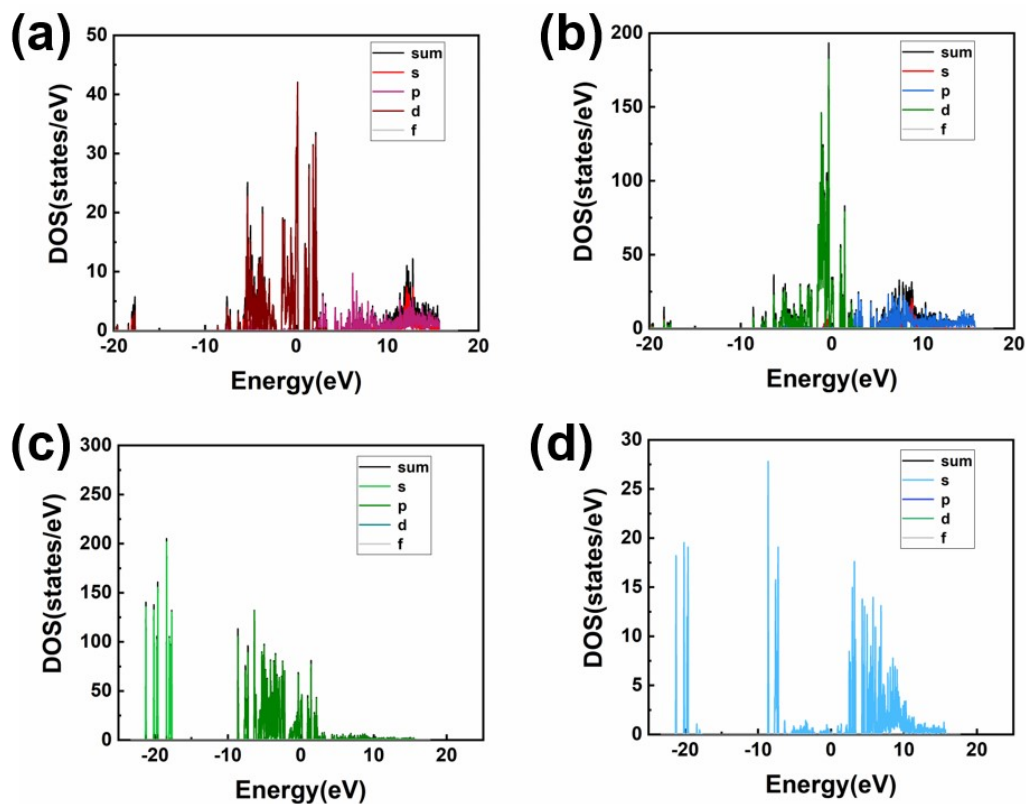**Figure S11**. Total and partial electronic density of states (TDOS and PDOS) calculated for (a) Fe, (b) Ni, (c) H and (d) O of NiFe-LDH.
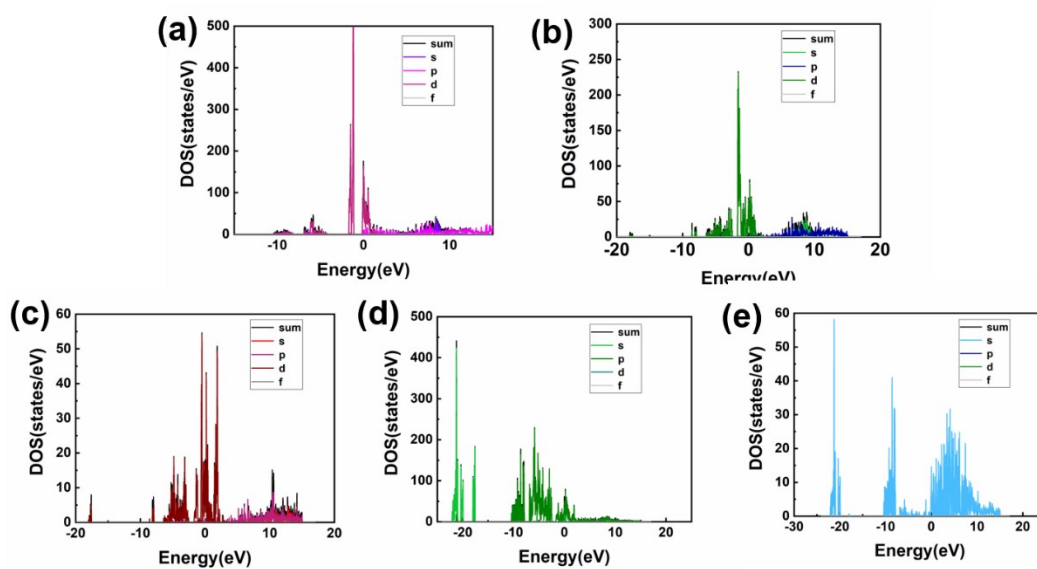


**Figure S12**. Total and partial electronic density of states (TDOS and PDOS) calculated for (a) Co, (b) Ni, (c) Fe and (d) H, and (O) of Co@NiFe-LDH.
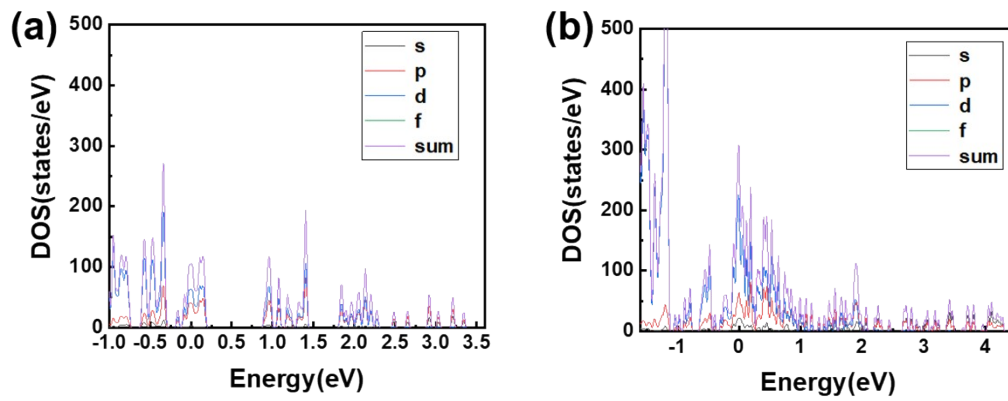
**Figure S13.** The partial density of states of (a) NiFe-LDH and (b) Co@NiFe-LDH.

## Supplementary Tables

**Table S1.** The content of Co, Ni, and Fe elements for all the samples, measured by inductively coupled plasma-atomic emission spectrometry (ICP-AES).

| Catalyst | Co (wt. %) | Ni (wt. %) | Fe (wt. %) |
|---|---|---|---|
| NiFe-LDH | — | 42.834 | 14.262 |
| CoNiFe-LDH | 9.645 | 38.531 | 9.156 |
| Co@NiFe-LDH | 9.873 | 38.463 | 9.267 |

**Table S2.** The OER performance comparison for non-precious-metal based electrocatalysts in 1.0 M KOH.

| Catalyst | $\eta$@10mA cm$^{-2}$ (mV) | Tafel Slope (mV dec$^{-1}$) | Reference |
|---|---|---|---|
| **Co@NiFe-LDH** | **253** | **44** | **This work** |
| NiCo$_2$S$_4$@NiFe-LDH | 287 | 86 | *Appl. Catal. B Environ.* **2021**, *286*, 119869 |
| S/NiN$_x$-PC/EG | 280 | 45 | *Nat. Commun.* **2019**, *10*, 1392 |
| $\alpha$-CoVO$_x$ | 347 | 97 | *ACS Catal.* **2018**, *8*, 644-650 |
| NiFeP/MXene | 287 | 86 | *Appl. Catal. B Environ.* **2021**, *286*, 119869 |
| CoP/NCNHP | 286 | 35 | *Sci. Bull.* **2021**, *66*, 1063-1072 |
| NiFe-LDH-0.4M HMS | 290 | 51 | *J. Energy Chem.* **2019**, *33*, 130-137 |
| CoP@PC-750 | 283 | 53 | *Small* **2019**, *15*, 1900550 |
| NiFe-OOHov | 288 | 38 | *Nano Energy* **2019**, *56*, 109 |
| CoP/TiOx | 337 | 72.1 | *Small* **2020**, *16*, 1905075 |
| Co$_2$P NRs | 372 | 111.8 | *J. Am. Chem. Soc.* **2020**, *142*, 8490 |
| FeNi$_3$@NC | 277 | 77 | *Appl. Catal. B Environ.* **2020**, *268*, 118729 |
| Ni-Fe$_2$O$_3$ | 277 | 68 | *ACS Sustainable Chem. Eng.* **2019**, *714*, 12117-12124 |

**Table S3.** The zinc-air battery performance comparison of the Co@NiFe-LDH decorated battery and other transition-metal-chalcogenide catalysts modified batteries.

| Catalyst | Peak power density (mW cm$^{-2}$) | Specific capacity (mA h g$^{-1}$) | Reference |
|---|---|---|---|
| **Co@NiFe-LDH** | **165** | **652** | **This work** |
| Zn-N-C-1 | 179 | 683 at 100 mA cm$^{-2}$ | *Angew. Chem.,* **2019**, *131*, 7109-7113 |
| Co-SAs@-NC | 105 | 897 at 20 mA cm$^{-2}$ | *Angew. Chem. Int. Ed.,* **2019**, *58*, 5359-5364. |
| Zn-Ni3FeN/NG | 158 | 650 at 20 mA cm$^{-2}$ | *J. Mater.Chem.A* **2021**, *9*, 2301-2307 |
| NiFe/NCNF/CC | 140 | 730 | *Appl. Catal. B Environ.* **2021**, *285*, 119856 |
| CNT-800 | 126.2 | 827 | *Appl. Catal. B Environ.* **2021**, *298*, 120511 |
| NFPC-1100 | 157 | - | *Appl. Catal. B Environ.* **2021**, *297*, 120448 |
| Cu/Zn-N$_4$ | 164.3 | - | *Small.* **2020**, *16,* 2004855 |

**Table S4.** Gibbs free energy change of the four elementary steps at different sites.

| Catalyst/site | Gibbs free energy change | | | |
|---|---|---|---|---|
| | $\Delta$ G1 | $\Delta$ G2 | $\Delta$ G3 | $\Delta$ G4 |
| NiFe-Ni site | 0.15994 | 1.78639 | 2.43197 | 0.5417 |
| NiFe-Fe site | 0.81375 | 1.04927 | 2.28207 | 0.77491 |
| Co@NiFe-Ni site | 1.81921 | 1.8253 | 1.76417 | -0.48868 |
| Co@NiFe-Fe site | 1.02299 | 1.40719 | 1.57897 | 0.91085 |